Delayed Parabolic Oxidation via Transient Thermal Exposures on a Polycrystalline Nickel-Based Superalloy

Wo, Jackson; Collins, David; Taylor, Mary; Hardy, Mark; Stone, Howard

Document Version
Version created as part of publication process; publisher's layout; not normally made publicly available

[Link to publication on Research at Birmingham portal](#)

Journal Pre-proof

Delayed Parabolic Oxidation via Transient Thermal Exposures on a Polycrystalline Nickel-Based Superalloy

J.W.X. Wo, D.M. Collins, M.P. Taylor, M.C. Hardy, H.J. Stone

Please cite this article as: J.W.X. Wo, D.M. Collins, M.P. Taylor, M.C. Hardy and H.J. Stone, Delayed Parabolic Oxidation via Transient Thermal Exposures on a Polycrystalline Nickel-Based Superalloy, *Corrosion Science*, (2023) doi:https://doi.org/10.1016/j.corsci.2023.111675

This is a PDF file of an article that has undergone enhancements after acceptance, such as the addition of a cover page and metadata, and formatting for readability, but it is not yet the definitive version of record. This version will undergo additional copyediting, typesetting and review before it is published in its final form, but we are providing this version to give early visibility of the article. Please note that, during the production process, errors may be discovered which could affect the content, and all legal disclaimers that apply to the journal pertain.

Delayed Parabolic Oxidation via Transient Thermal Exposures on a Polycrystalline Nickel-Based Superalloy

J. W. X. Wo [a], D. M. Collins [b], M. P. Taylor [b], M.C. Hardy [c], H. J. Stone [a,*]

[a] Department of Materials Science and Metallurgy, University of Cambridge, 27 Charles Babbage Road, Cambridge, CB3 0FS, UK
[b] School of Metallurgy and Materials, University of Birmingham, Pritchatts Road, Birmingham, B15 2TT, UK
[c] Rolls-Royce plc, PO Box 31, Derby, DE24 8BJ, United Kingdom
*Corresponding author. Tel.: +44 (0)1223 334320, Email: hjs1002@cam.ac.uk

Abstract

Multiple oxides were observed during the transient oxidation stage of the polycrystalline Ni-based superalloy, RR1000, before a protective Cr_2O_3 scale formed. Thermogravimetric analysis, synchrotron grazing incidence X-ray diffraction, and electron microscopy were performed on samples subjected to isothermal exposures at 800 °C for up to 100 hours. Transient effects governed the early stages up to 40 hours. NiO, spinels ($NiCr_2O_4$, $(Ni,Co)(Cr,Co)_2O_4$), $Cr_2O_3/(Cr_{0.88}Ti_{0.12})_2O_3$, $NiTiO_3$, and $CrTaO_4$ formed during the initial stage with pseudo-linear kinetics. At the onset of parabolic kinetics, extensive Cr_2O_3 and TiO_2 growth dominated scale formation with the former emerging as the major passivating oxide.

Keywords

nickel, superalloys, X-ray diffraction, SEM, oxidation

1 Introduction

Historical superalloy development [1] has resulted in many commercially successful polycrystalline Ni-based superalloys, e.g. Waspaloy, IN 718, Udimet 720, Alloy 625, and RR1000. The high temperature oxidation of polycrystalline superalloys typically results in the formation of an external compact scale of Cr_2O_3, with discontinuous finger-like intrusions of Al_2O_3 in the subscale [2–4]. In addition to Cr and Al, the complex compositions of these alloys can lead to the formation of multiple oxides. For example, one study investigated the oxidation of several commercial polycrystalline Ni-based superalloys from 750-1000 °C and showed that Al only formed internal oxides, whilst Cr and Ti formed external oxides that resulted in complex multi-layered oxide scales [2]. Similar results [5] were observed in alloys of varying Al, Co, Cr, and Ti concentrations where internal Al_2O_3 formed, with significant layers of Co, Cr, and Ti-based oxides on the external surface. The study also showed that the capacity of the alloys to form a continuous Cr_2O_3 layer could be improved by decreasing Co or Ti and increasing Al or Ni concentrations. For the Ni-based superalloy RR1000, significant enrichment of Cr and Ti in the external scale formed at 600-900 °C has been observed consistently in multiple studies [6–9]. It has also been shown that Cr and Al work synergistically to form a multi-layered oxide scale, with the former promoting the formation of the latter [10]. These studies suggest that Cr and Al concentrations must be carefully selected to achieve optimal environmental resistance. Further studies have also shown that the growth kinetics of Cr_2O_3, specifically, can be influenced by other alloying additions via doping, for instance [5,8,11–14], and also by the formation of stable phases that tie up the dopant within the alloy and thus reduce the impact [15,16].

Transient oxidation in Ni-based alloys occurs where different oxides form before the eventual ascendancy of more stable oxides (e.g. Cr_2O_3) once steady-state isothermal oxidation is achieved after prolonged

exposure to elevated temperatures [17]. This primarily arises due to the competing reactions between the various alloying elements with adsorbed oxygen anions during initial exposure to the oxidising environment. In general, identifying the oxides formed during transient oxidation can be difficult given their small volumes and varying timescales of formation as well as the possible spallation of non-adherent oxide products. Several studies into the transient oxidation stages on Ni-based alloys have shown the early formation of NiO on the alloy surface [4,18–20], due to the high Ni concentration in the alloy and the faster oxidation kinetics relative to the other potential oxides [21]. Another group of oxides that form during transient oxidation are the spinels, which have the formula of AB_2X_4 where A is typically Ni, B is Co, Cr, Ta or Al, and X is O [17,22]. Several mechanisms leading to the formation of spinels have been proposed [23–26]. Moreover, the precise role of spinels in the transient and long-term steady-state oxidation regimes is controversial. While generally considered to be non-protective oxides that form discontinuous scales, it has been reported that the presence of spinel oxides could also have beneficial effects on the oxidation resistance of superalloys [27–29]. It can be rationalised that the formation of spinels during the transient oxidation phase could act as barriers to oxygen ingress, giving sufficient time for a more stable oxide (e.g. Cr_2O_3) to form as a result of the reduced partial pressure of oxygen at the oxide-metal interface. However, the absence of a reliable method to monitor transient oxidation processes in real-time makes it challenging to confirm this theory.

It is acknowledged that thin oxide scales formed on the alloy surface, compared to the volume of the underlying bulk alloy substrate, can be problematic to characterise with conventional X-ray diffractometry (XRD) due to inherently low volume fractions. Under such circumstances, the early onset and evolution of oxide products can be difficult to detect. However, a recent study of thin oxide scales with synchrotron X-ray diffraction [25] has shown promise to successfully characterise the oxide products during transient oxidation since the high intensities of the incident beam allow for the detection of even low-volume fraction phases. Moreover, high-sensitivity thermo-gravimetric analysis (TGA) equipment has also been shown [30] to be capable of detecting subtle changes in kinetics. This level of accuracy has enabled the development of algorithms to account for the formation of oxides and their interplay [30].

It is clear from the literature that the oxidation behaviour of Cr_2O_3-forming polycrystalline Ni-based superalloys is well-understood. In particular, the commercial superalloy RR1000 has been extensively studied and therefore provides an excellent opportunity for establishing an understanding of oxidation dynamics in polycrystalline Ni-based superalloys. The present study outlines the oxidation behaviour of RR1000 up to 100 hours at 800 °C with a focus on the transient oxidation stage. To study this behaviour, oxidation tests were performed on samples subjected to systematically increasing exposure times following a controlled heating stage. The results are compared with data from previous studies.

2 Material and Methods

2.1 Materials
The composition of coarse-grained RR1000, an established polycrystalline Ni-based superalloy used in turbine disc applications with a nominal grain size of approximately 30 μm [31], is outlined in Table 1. Samples were obtained from a test ring of a high-pressure turbine front cover plate forging, provided by Rolls-Royce plc. The test ring was commercially solution heat treated at 1170 °C for 1 hour, followed by a precipitation ageing heat treatment at 760 °C for 16 hours.

Table 1 – Nominal and actual compositions of RR1000 (at.%). It was not possible to accurately measure the actual concentrations for B and C with Energy Dispersive X-ray (EDX) and therefore these values were omitted from the table. Adapted from [32].

	Ni	Co	Cr	Al	Ti	Ta	Hf	Zr	Mo	B	C
Nominal	50.96	17.90	16.50	6.30	4.30	0.63	0.16	0.04	3.00	0.08	0.13
Actual	49.82	18.19	17.23	6.15	4.50	0.88	0.13	0.04	3.07	-	-

The actual composition of RR1000, as given in Table 1, was measured with Energy Dispersive X-ray (EDX) analysis and averaged over three representative regions with approximate field-of-view dimensions of 23 x 18 μm^2 and an acquisition time of 10 minutes per region. In general, the results showed reasonable agreement between the actual and nominal compositions.

2.2 Oxidation Tests

TGA measurements were performed using a Setaram Setsys Evolution 18 apparatus to study the specific mass change associated with oxidation for RR1000 at 800 °C for 0 (the experiment was stopped immediately after the heating stage), 10, 20, 40, 60, 80, and 100 hours isothermal exposure in air. A testing temperature of 800 °C was selected to replicate the upper limit of operating temperatures that are typically expected for turbine discs. Samples for TGA analysis were prepared with approximate dimensions of 20 x 10 x 1 mm^3. The final sample dimensions were measured using a digital vernier scale to allow specific mass changes to be calculated from associated mass change data. All faces and sides of the samples were polished to a 1 μm diamond finish. Before the TGA experiments, samples were cleaned in acetone followed by ethanol in an ultrasonic bath and dried for at least 24 hours in a drying cabinet. During the heating process, the sample was first heated from 20-200 °C at 10 °C/min and held for 10 minutes to stabilise. The sample was then heated from 200-775 °C at 20 °C/min. To avoid overshooting the temperature, the sample was heated from 775-800 °C at 5 °C/min. During the cooling process, the sample was cooled from 800 °C to 20 °C at 35 °C/min.

For the 100-hour oxidation test, the oxidation rate constant and mass gain exponent were acquired by fitting to a generalised form of the classical power law equation using the MATLAB Curve Fitting Tool:

$$(\Delta m)^n = k_n t \qquad (1)$$

where Δm is the specific mass change (mg/cm^2), k_n is the oxidation rate constant (mg^n/cm^{2n}h), and t is the time (h). Parabolic oxidation behaviour is represented by an $n \approx 2$, indicating that the growth is governed by diffusion of the oxidising species through the oxide. The 95% confidence bounds on the fitted coefficients were also computed with the MATLAB Curve Fitting Tool using Student's cumulative t-distribution function.

2.3 Synchrotron X-ray Diffraction Experiments

Synchrotron grazing incidence X-ray diffraction (SGIXD) was used to characterise the thin oxides formed during the thermal exposures. This technique provides very high angular resolution, high intensity and low instrumental peak broadening compared to conventional laboratory-based diffractometry, which greatly facilitates the identification of the phases present even at low-volume fractions. In this study, the procedure reported in [25] was employed and a schematic illustration of the setup geometry is provided in Figure 1. The incident beam was inclined to the sample surface by an angle of 1 ° so that the resulting diffraction signal probes only the top few micrometres of the sample, making it advantageous for oxide analysis on the

surface of the RR1000 samples. The SGIXD method was performed at the I11 high-resolution powder diffraction beamline at the Diamond Light Source, UK.

The X-ray measurements were acquired with a monochromatic 15 keV incident beam energy (with an equivalent wavelength of 0.8264 Å), which was calibrated against a NIST 640c Si standard. Each sample was mounted onto the sample stage of the diffractometer using a carbon tab. Diffraction patterns were acquired over a 3-150° 2θ scan range using the high-resolution multi-analysing crystals (MAC) detector (the primary detector on the I11 beamline). The scan time for each sample was 30 minutes, collected with an angular increment of 0.001°, determining the angular resolution. To improve the signal-to-noise ratio, the data was re-binned into 0.02° intervals.
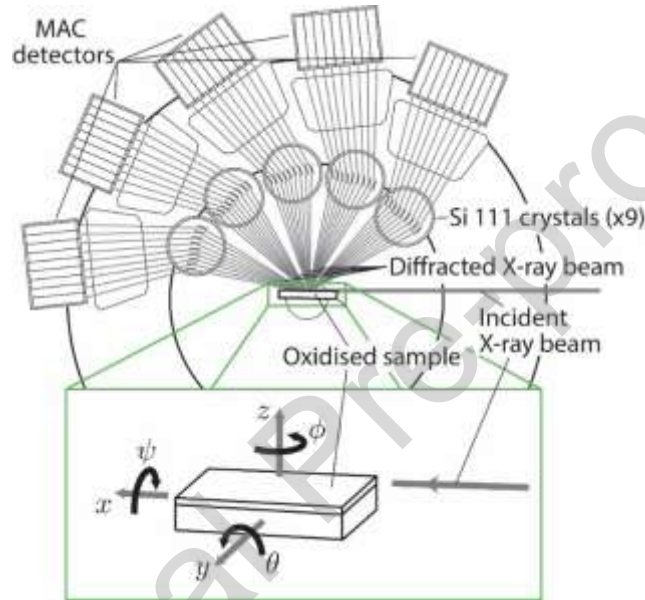

Figure 1 - Schematic illustration of the SGIXD configuration used on the I11 beamline. An incident beam was impinged on the surface of the sample with the diffracted X-rays being fed through Si 111 crystals and received by multi-analysing crystals (MAC) detectors. Directions and rotational axes with respect to the incident beam and sample are also shown. Image adapted from [25] with permission.

2.4   Oxide Analyses

Samples for oxide examination were Ni-plated for oxide preservation and sectioned with a precision saw utilising a SiC blade. A low-impact dry-cut method was used to minimise potential damage to the oxide layers. The sectioned samples were cold mounted in resin and subsequently ground down by at least 1 mm using SiC grinding papers to ensure the prepared oxide cross-sections were free from any cutting damage. Samples were polished to a 0.06 μm colloidal silica suspension finish. Samples were attached to an SEM stub using Cu-tape for enhanced conductivity during Scanning Electron Microscope (SEM) examination.

Microstructural examination of the polished cross-sections was carried out in a Zeiss GeminiSEM 300 SEM operated at 20 kV and a working distance of approximately 8.5 mm. The instrument was also equipped with an Oxford Instruments EDX detector to facilitate compositional analyses of microstructural features. Oxide cross-sections were examined in Backscattered Electron (BSE) mode and EDX elemental concentration maps of the alloy cross-sections were acquired alongside BSE SEM micrographs.

To investigate the evolution of the oxides and phases with increasing time, a general Rietveld analysis was performed on the SGIXD data using TOPAS-Academic V6 software [33]. Rietveld refinement of the data

allowed for the determination of individual phase fractions from the detected oxides. To this end, relevant CIF files were acquired from the Inorganic Crystal Structure Database (ICSD) through the Physical Sciences Data-Science Service (PSDS) [34]. In addition, the appropriate instrumental parameters for the I11 beamline were acquired from the Diamond Light Source. The RR1000 sample that was oxidised at 800 °C for 100 hours was expected to possess the greatest quantity of surface oxides and was therefore deemed to be the most amenable for Rietveld analysis and, as such, was refined first. Once a satisfactory fit was achieved, its weighted profile R-factor (R_{wp}) was used as an approximate guide in the refinement of subsequent datasets. By subjecting each dataset to a similar level of refinement, it was possible to identify trends in the data when investigating the transient oxides formed.

3   Results

3.1   Thermo-Gravimetric Analysis

The specific mass changes recorded using the TGA instrument for RR1000 during isothermal oxidation at 800 °C for 0-100 hours are presented in Figure 2. A zoomed-in view of the first 30 hours is shown in Figure 3. During the initial 30-40 hours of oxidation, the specific mass change curve for RR1000 had an approximately linear profile. Beyond ~40 hours, the curves followed a parabolic profile. The specific mass change curves for RR1000 were reproducible and virtually identical in the early stages.
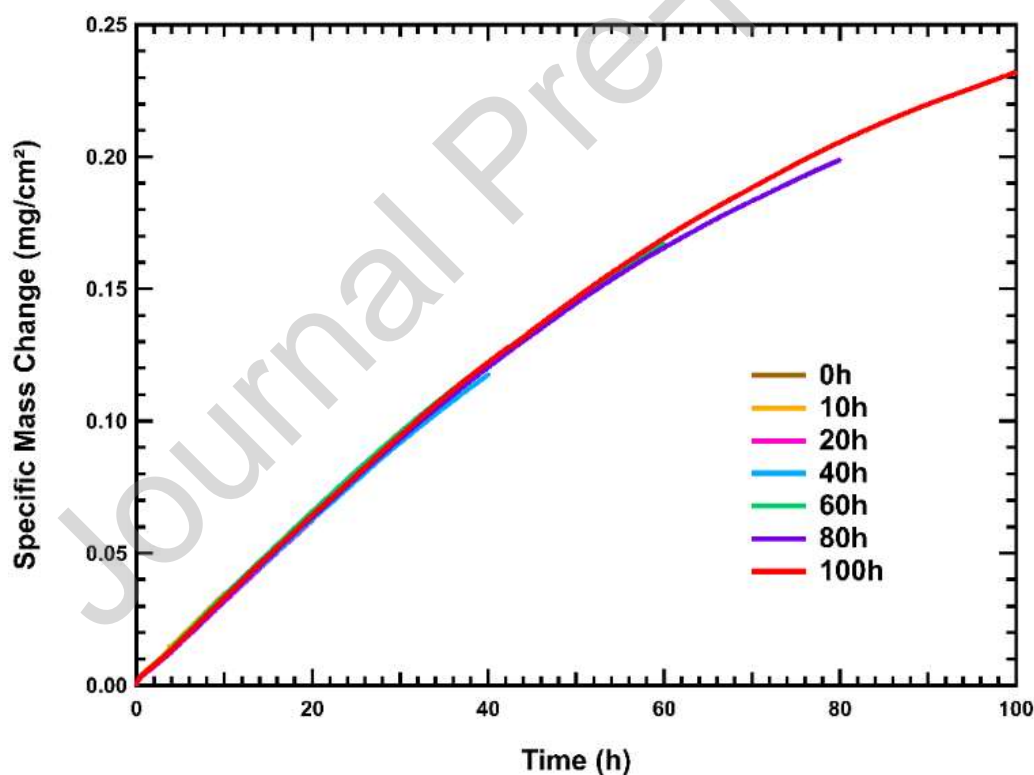

Figure 2 - TGA specific mass change curves for isothermal oxidation of RR1000 samples for times up to 100 hours at 800 °C in air. A separate sample was exposed for each period outlined in the legend. The traces show a period of approximately linear kinetics up to 40 hours followed by a decreasing oxidation rate.
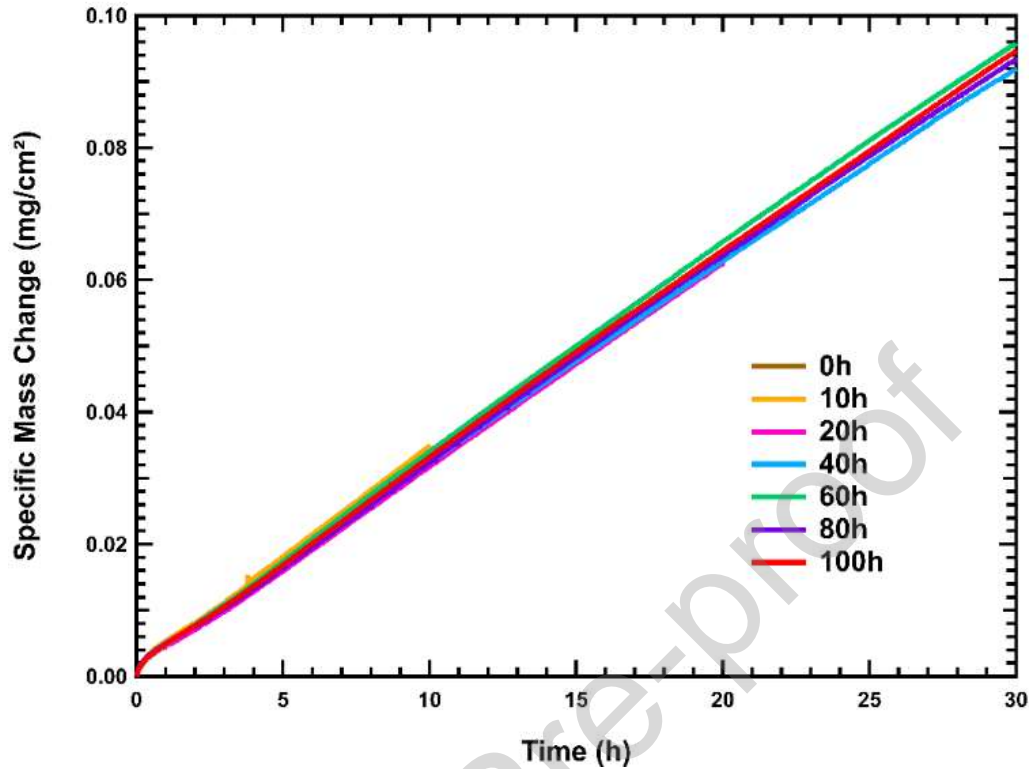
Figure 3 - TGA specific mass change curves for isothermal oxidation of RR1000 samples at 800 °C over the time period of 0-30 hours in air showing linear or near-linear growth kinetics.

The fitted mass change coefficients from Equation (1) for the 100-hour exposure at 800 °C are given in Table 2 with 95% confidence bounds in parentheses. For comparison with literature values, the data were also fitted to an $n = 2$. Where parabolic kinetics was assumed, n is expressed as "2.000". Assuming parabolic behaviour, the k_n value for RR1000 in this study was similar to that reported in the literature, as shown in Table 2.

Table 2 - Values of n and k_n from Equation (1) determined for RR1000 after oxidation at 800 °C for 100 hours with 95% confidence bounds in parentheses. Literature values are provided for comparison and sources are given.

	This Study		**Taylor et al.** [9]	**Encinas-Oropesa et al.** [35]	**Cruchley et al.** [7]	**Cruchley et al.** [8]
n	1.286 (1.284, 1.289)	2.000	2.000	2.000	2.000	2.040
k_n ($\times 10^{-4}$) ($mg^n/cm^{2n}h$)	16.23 (16.16, 16.30)	4.560 (4.538, 4.581)	6.696	9.120	4.572	4.392
Test Period (h)	100	100	100	200	2000	2000

3.2 SGIXD Analysis

The SGIXD diffractograms obtained from the surface oxide scales of RR1000 after exposure at 800 °C for 0-100 hours following the heating stage are shown in Figure 4. Strong diffraction peaks corresponding to the γ matrix and γ′ precipitation phases in RR1000 could be identified, which dominated the diffraction signal from the 0-hour sample. Peaks associated with NiO, Cr_2O_3, $NiCr_2O_4$ (tetragonal), TiO_2, $(Cr_{0.88}Ti_{0.12})_2O_3$, $(Ni,Co)(Cr,Co)_2O_4$, $NiTiO_3$, and $CrTaO_4$ oxides were also identified. It is noted that $NiCr_2O_4$ has a cubic structure at high temperatures but transforms to a tetragonal structure below 46°C [36]; each allotrope can be distinguished from other phases present. Due to the significant similarities in crystal structure and lattice parameters for the cubic spinels, these compounds are referred to herein the general form $(Ni,Co)(Cr,Co)_2O_4$.

The spectra for the oxide phases showed clear and systematic increases in intensity with increasing time of exposure, which is most prominent in the approximate 13, 15, 18, 19, 22, and 32.5/33° 2θ positions. In contrast, the spectra for the γ and γ′ phases showed systematic decreases in intensity with increasing time of exposure as evidenced by the approximate 38, 45, 47, 60, and 62° peak locations.

Figure 4 - Synchrotron grazing incidence X-ray diffractograms (SGIXD) from the surface of RR1000 after oxidation at 800 °C for 0-100 hours in air.

Rietveld refinement was performed on the SGIXD data in Figure 4 and the corresponding fits are shown in Figure 5 on a square root intensity scale. To compare the fidelity of the refinements, the difference between the experimental data and the calculated fit (i.e. residual) is shown for each experimental run. For some peak locations, it was challenging to describe the intensity of the experimental data with the calculated fits which resulted in slight underfitting. However, the residuals were considered small and demonstrated good agreement between the experimental data and the calculated fits.

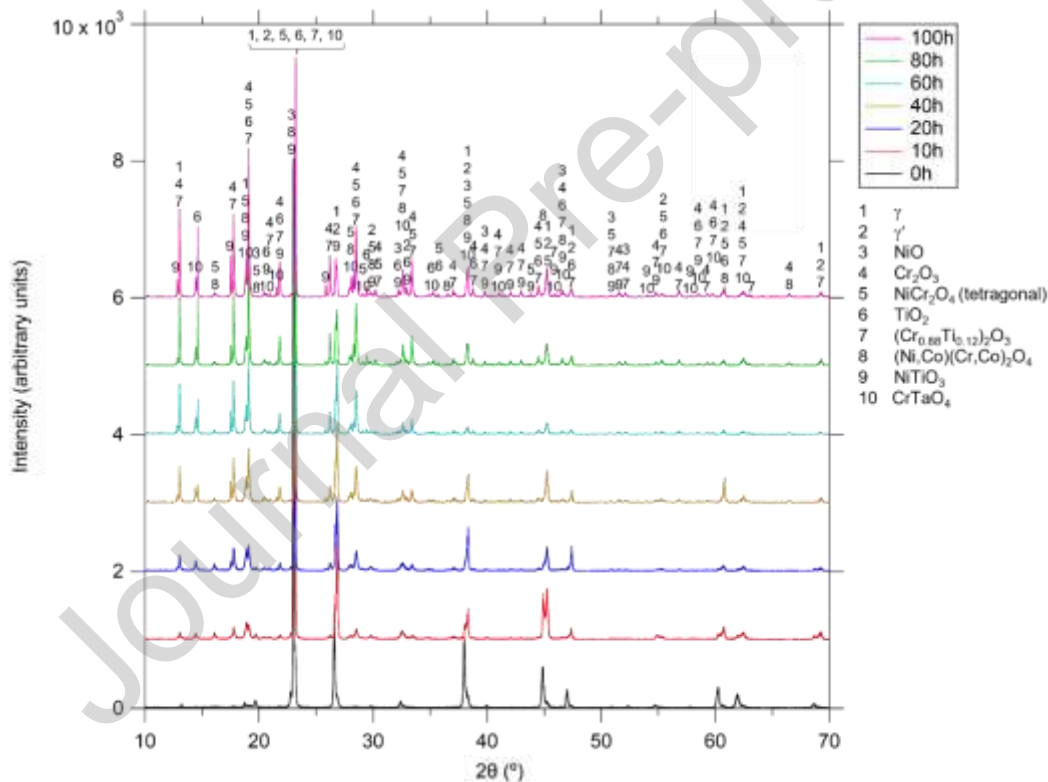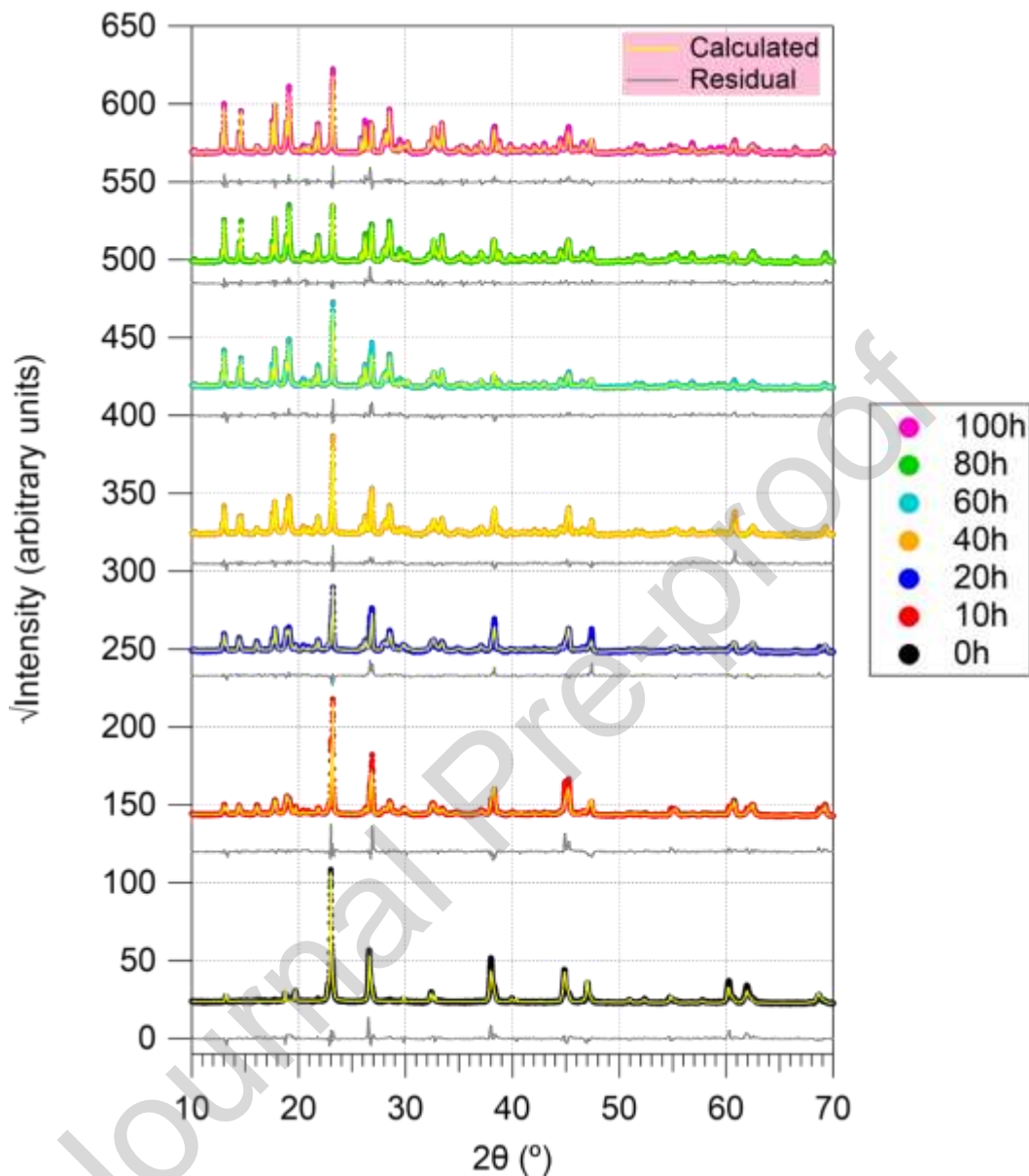*Figure 5 - Calculated fits and residuals using Rietveld refinement of synchrotron grazing incidence X-ray diffractograms (SGIXD) from the surface of RR1000 after oxidation at 800 °C for 0-100 hours in air.*

Individual phase fractions (wt.%) obtained from the Rietveld refinements using TOPAS-Academic V6 software were used to examine the evolution of the identified phases as a function of time at 800 °C and are displayed in Figure 6. The SGIXD spectra were initially dominated by signals attributed to the γ, γ', and NiO phases. The first 0-10 hours were characterised by a reduction of NiO followed by increasing formation of spinels ($NiCr_2O_4$ (tetragonal)/$(Ni,Co)(Cr,Co)_2O_4$) and Cr_2O_3/$(Cr_{0.88}Ti_{0.12})_2O_3$ while γ and γ' fractions decreased. From 10-40 hours, Cr_2O_3/$(Cr_{0.88}Ti_{0.12})_2O_3$ grew to become the major oxide while significant fractions of $NiTiO_3$ and $NiCr_2O_4$ (tetragonal) were also present. The amount of NiO decreased almost completely to zero during the first 30 hours. From 40 hours onward, Cr_2O_3 and TiO_2 were the major oxides present alongside $(Cr_{0.88}Ti_{0.12})_2O_3$ and $NiTiO_3$. The cubic spinels, $(Ni,Co)(Cr,Co)_2O_4$, also decreased in

fraction over this time period while that of $NiCr_2O_4$ (tetragonal) remained stable. It is noted that a separate sample was prepared for each oxidation test and therefore some sample-to-sample variation may be present.
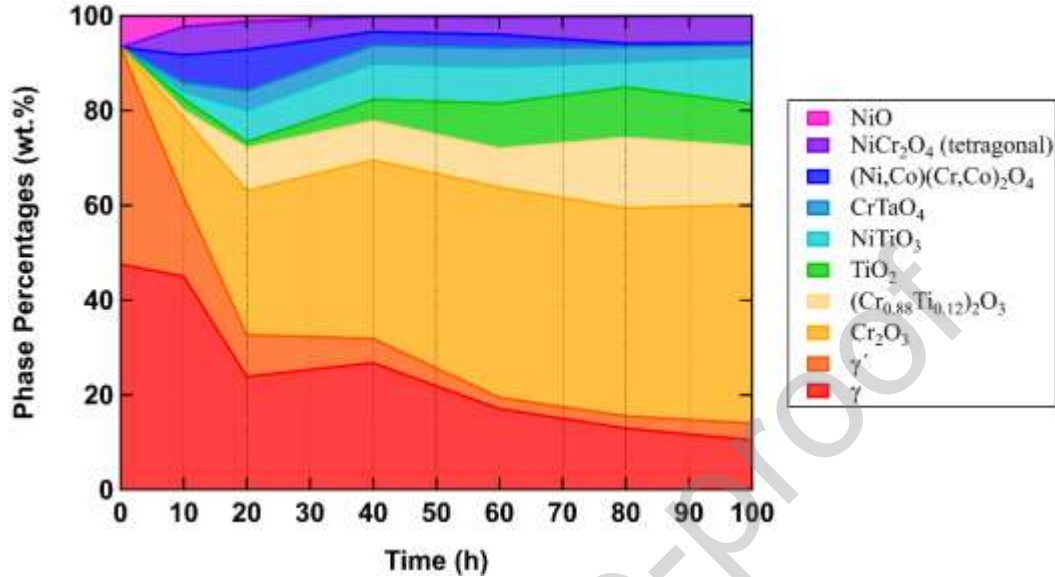

Figure 6 - Evolution of phase fractions (wt.%) calculated with Rietveld refinement of synchrotron grazing incidence X-ray diffractograms (SGIXD) from the surface of RR1000 after oxidation at 800 °C for 0-100 hours in air.

The identified phases in Figure 4 and fractions in Figure 6 are tabulated in Table 3 with associated uncertainties calculated using TOPAS-Academic V6. In addition, the relevant CIF file code for each phase used and the weighted profile R-factor (R_{wp}) for each Rietveld refinement are shown.

Table 3 - Identified phases in RR1000 during oxidation at 800 °C for 0-100 hours following the heating stage. CIF collection codes for each phase are provided. The uncertainties and R_{wp} values for each Rietveld refinement calculated in TOPAS-Academic V6 are also shown.

Phase (wt.%)	CIF Code	0h	+/-	10h	+/-	20h	+/-	40h	+/-	60h	+/-	80h	+/-	100 h	+/-
γ	53807	47.5	0.8	45.0	1.6	23.9	0.8	26.7	0.6	17.1	0.5	13.0	0.3	10.4	0.2
γ'	58039	45.8	0.8	16.8	0.9	8.8	0.4	5.1	0.3	2.4	0.3	2.6	0.2	3.6	0.2
Cr_2O_3	75577	-	-	16.8	1.4	30.4	1.5	37.7	1.1	44.4	1.1	43.9	0.9	46.1	0.8
$(Cr_{0.88}Ti_{0.12})_2O_3$	74195	-	-	1.4	1.4	9.0	1.7	8.2	1.2	8.2	0.9	14.9	0.9	12.2	0.8
$NiCr_2O_4$	280062	-	-	6.0	1.4	5.9	1.1	3.2	0.6	3.6	1.0	5.7	0.5	5.8	0.3
TiO_2	167955	-	-	2.5	1.0	1.3	0.4	4.5	0.4	9.5	0.5	10.7	0.4	9.1	0.4
$(Ni,Co)(Cr,Co)_2O_4$	8679 61612	-	-	5.8	1.2	8.6	0.9	2.8	0.5	2.8	0.9	0.7	0.3	0.4	0.2
$NiTiO_3$	171584	-	-	1.5	0.5	6.6	0.6	7.6	0.4	7.7	0.4	5.3	0.2	9.8	0.3

CrTaO₄	247441	-	-	2.0	0.5	4.2	0.3	3.9	0.2	4.0	0.3	3.2	0.1	2.6	0.1
NiO	259698	6.6	0.3	2.3	0.5	1.2	0.2	0.2	0.1	0.3	0.3	0.2	0.1	0.0	0.0
R$_{wp}$		27.5		28.7		22.9		19.4		24.8		18.1		20.5	

3.3   Cross-Sectional Oxide Analysis

BSE SEM images of RR1000 cross-sections and associated EDX elemental concentration maps after exposures at 800 °C in air for 0-100 hours are presented in Figure 7. In the initial case (0 hours of isothermal exposure following the heating stage), the oxide scale on the surface of RR1000 was too thin to be positively identified using SEM EDX. It was noted that the Ni plating appeared to have separated from the oxide surface which could potentially have resulted in some oxide scale loss. Oxygen was detected, however, the exact composition of the oxide formed could not be measured using SEM EDX. As the relative amounts of Ni in the alloy and NiO are similar, it is postulated that the most likely oxide formed is that of Ni, as revealed by the SGIXD above. After 10 hours, early oxidation products were visible near the surface which EDX showed as predominantly Cr and Ti oxides. The thickness of the oxide formed varied across the surface of the sample with faster growth noted at emergent grain boundaries, identifiable by the presence of internal oxidation (finger-like intrusions) of Al. After 20 hours, a more continuous external scale of Cr_2O_3 was beginning to form across the surface of the sample with internal Al_2O_3 intrusions. The thickness of the surface layer of Cr_2O_3 after this period of exposure continued to show non-uniform growth, with the faster oxidation kinetics shown at emergent grain boundaries. The presence of TiO_2 in the external scale was observed and an obvious Ti-depleted zone developed with the alloy beneath the external scale. Similar to the 0-hour sample, the Ni plating appeared to have separated from the oxide surface and may have also resulted in some oxide scale loss. After 40 hours, the external Cr_2O_3 scale had thickened on the surface of the alloy. After 60 hours, the Cr_2O_3 scale remained relatively constant while TiO_2 increased in thickness. Moreover, the Ni plating appeared to have separated from the oxide scales and a significant amount of compacted debris from the grinding/polishing procedure was entrapped in the resulting gap. However, this does not appear to have adversely affected the Cr_2O_3 and TiO_2 scales as these are still distinguishable from the debris. The thickness of the Cr_2O_3/TiO_2 scale did not increase markedly from 80 to 100 hours, but the size and depths of the discontinuous Al_2O_3 intrusions increased and continued to extend into the alloy. While no specific areas of significant Co and Ni concentrations were observed, faint protrusions enriched in Co and Ni were detected at the alloy surface. Regions of Mo enrichment were also observed near the surface of the alloy and surrounding the Al_2O_3 intrusions. No significant Ta enrichment was observed in the initial condition but gradually increased in intensity from 10-40 hours, reaching an approximately constant thickness from 60-100 hours.
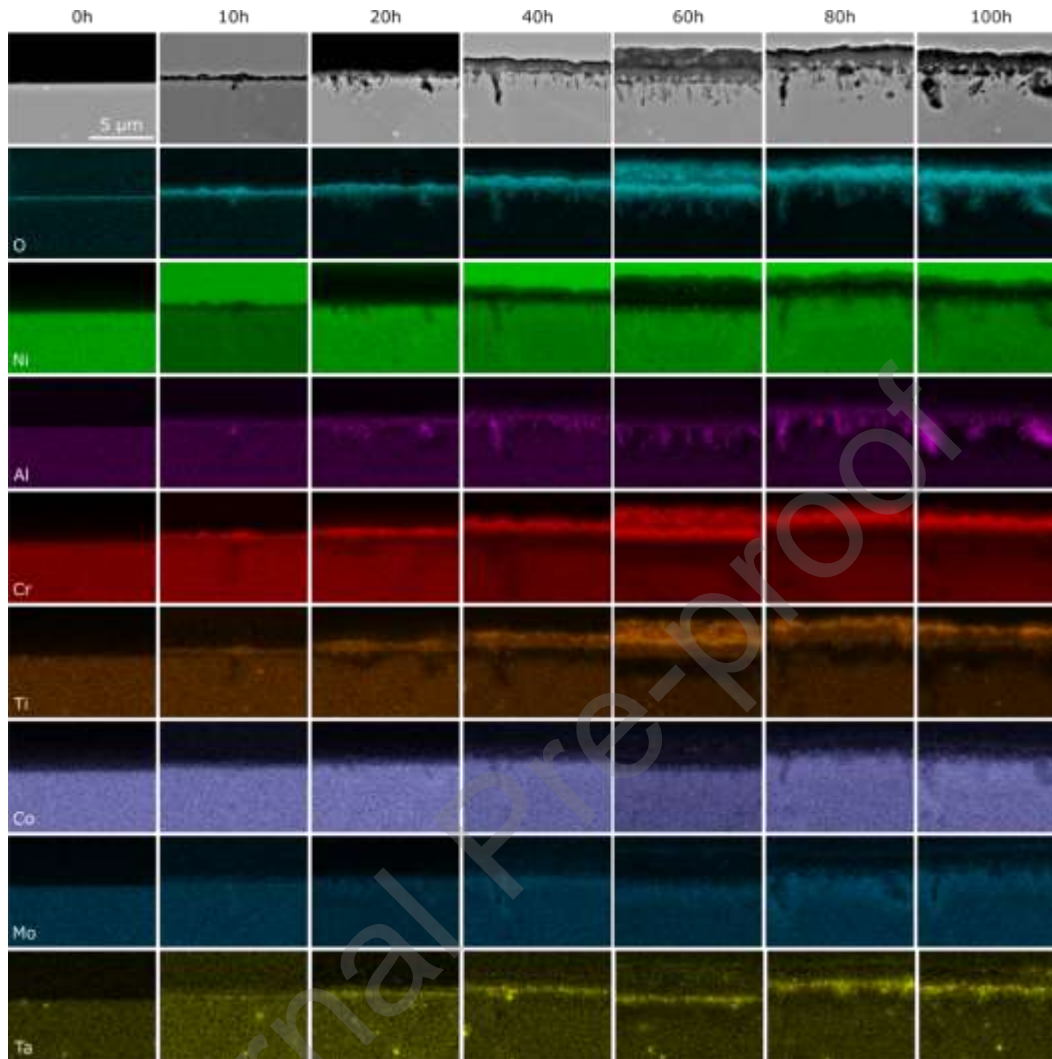
Figure 7 - Cross-sectional BSE SEM images (top row) and corresponding EDX elemental concentration maps of RR1000 after oxidation at 800 °C for 0-100 hours in air. It is noted that the Ni plating had separated from the oxide scales in the 0-hour, 20-hour, and 60-hour samples. The 60-hour sample showed compacted debris from grinding and polishing procedures entrapped in the gap between the oxide scales and detached Ni plating.

4 Discussion

4.1 Thermo-Gravimetric Analysis

The TGA results in Figure 2 and Figure 3 showed approximately linear specific mass change kinetics over the early oxidation stages of RR1000 at 800 °C (up to 30-40 hours) followed by decreasing oxidation rates. This change in kinetic law with increasing time at temperature contrasts with previous studies where parabolic kinetics were recorded from the outset of isothermal exposure [9,35]. A value for n of 1.286 was determined for the collected data (Figure 2 and Figure 3) and suggests a kinetics relationship that is closer to linear than parabolic. The earlier studies found the alloy, at 800 °C, followed parabolic kinetics over the same time period, i.e. up to 100 and 200 hours, respectively [9,35]. The difference between the results obtained in this study and those of the similar studies on the same alloy was unexpected. The linear kinetics recorded in this study up to 40 hours showed a prolonged period of transient oxidation before the protective

and continuous scale of Cr_2O_3 had been established. The EDX results in Figure 7 revealed the development of the oxides on the alloy surface. At 0 hours (i.e., following the heating rate), oxygen was detected at the surface of the alloy, with SGIXD confirming this to be NiO. At 10 hours, a discontinuous Cr_2O_3 scale had formed along with TiO_2, corresponding to the onset of linear kinetics as shown in the TGA results. It is believed that the formation of these two oxides, the observed differences in growth rate across the surface of the samples, and the additional identified oxides contributed to the linear kinetic region of the TGA results. It was also noticeable that the concentration of NiO decreased over this time period. At 40 hours, the EDX maps showed a continuous Cr-rich oxide had formed at the surface of the alloy and the majority of the additional oxides were found using SGIXD to be either stable in concentration or decreasing in intensity. At 40 hours, a classical parabolic profile began.

The difference in the value of n in this study to that reported in [9,35] could be explained by examining the specific protocol details of the testing performed. The heating rate used in this study is presented in Figure 8 along with the heating rates used in the systematic study by Reynolds et al. [25] which investigated the effect of heating rates (2, 5, 10, 20, 40, 100 °C/min) from ambient conditions to a test temperature of 650 °C on the oxidation of RR1000. The average heating rate in this study is approximately 13 °C/min and is therefore between the 10 °C/min and 20 °C/min heating rates observed in [25]. Thus, in this study it took approximately 1 hour for the samples to reach the test temperature of 800 °C, enabling a significant quantity of oxide formation to occur over the thermal transient stage. In this regard, the results agree with [25] where the formation of NiO and $(Ni,Co)(Cr,Co)_2O_4$ spinels were observed. Therefore, the oxides formed during the heating stage may have contributed to the relatively linear kinetics observed over the time period of up to 40 hours. However, it is noted that the test temperature was 650 °C in [25] while this study was conducted at 800 °C. It is possible that a faster heating rate may limit the extent of the transient oxidation stage in this alloy.
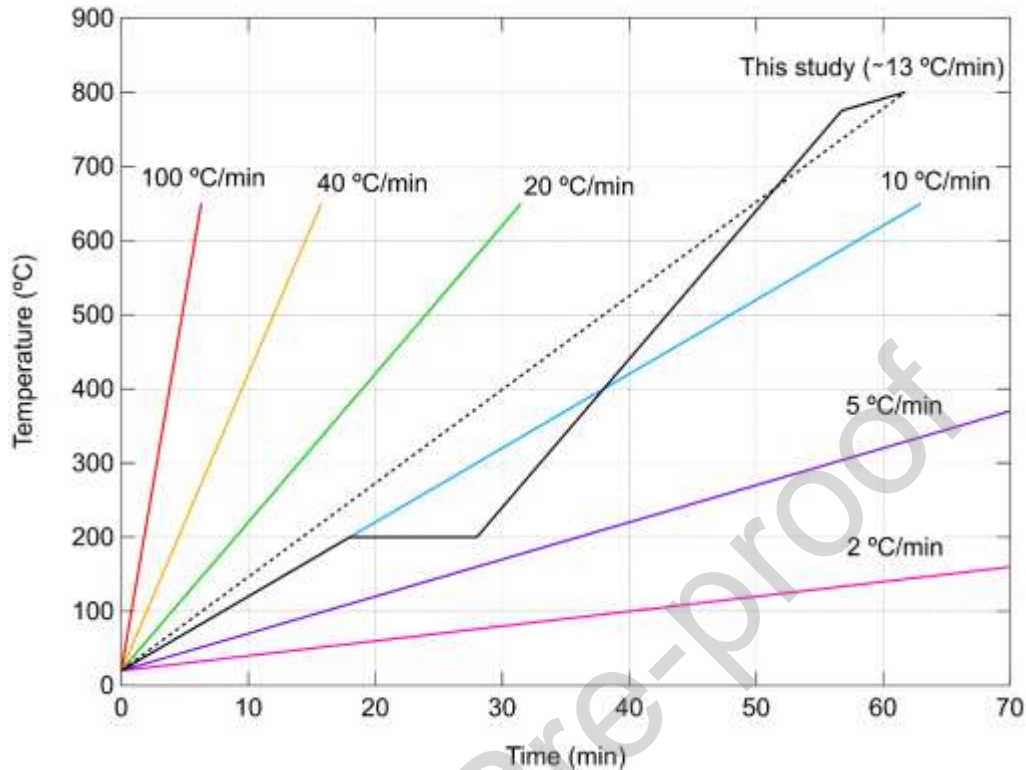
Figure 8 - Heating rates of RR1000 in a thermo-gravimetric apparatus. The heating profile used in this study (black) and the average heating rate (dotted) are shown alongside heating rates investigated in
[25].

In addition to the heating rates, the different surface finishes adopted in other studies compared to this investigation must be considered as they may influence the oxidation behaviour. The sources in Table 2 [7,8,35] had polished samples to either 0.25 μm or 6 μm diamond surface finishes which differ from the samples in this study (1 μm diamond finish). However, the final mass gain in Figure 2 shows close agreement with the final mass gain at 800 °C in [9], which suggests that the surface roughness range quoted for these studies does not significantly affect the overall mass gain. It has been proposed [37] that higher surface roughness can reduce oxidation damage and mass gains. It is theorised that the increased concentration of defects at the surface due to a higher roughness could create fast diffusion paths for Al or Cr, expediting protective oxide formation [37]. This hypothesis could explain why the results in [7,8] showed comparatively better (i.e. parabolic) kinetics than the present study. However, the reason why the result in [35] also showed parabolic kinetics despite having a smoother surface finish than the present study suggests that the different heating rates used may be the cause of the difference in the observed kinetics laws.
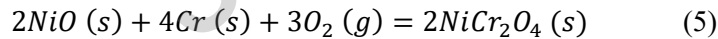
4.2 Temporal Evolution of Oxides

From the studies by Giggins and Pettit [4], the Ni, Cr, and Al content of this alloy (approximately Ni-16Cr-3Al wt% or Ni-17Cr-6Al at%) should form a continuous surface scale of Al_2O_3 instead of Cr_2O_3. This difference in behaviour can be attributed to the lower temperature used in this study, reducing the diffusion rate of Al [38]. Indeed, the increased diffusion rate of Al at higher temperatures has been used to promote Al_2O_3 formation on a Cr_2O_3-forming superalloy through high-temperature pre-oxidation treatments [39]. In addition, the role of the other alloying elements also needs to be considered. Critically, Ti additions have been shown to promote Cr_2O_3 scale formation in Ni-based alloys and suppress Al_2O_3 [15] through

accelerated Cr_2O_3 growth kinetics [8,11–14]. Conversely, in alloys where more stable phases containing Ti can form, lower Cr_2O_3 kinetics have been recorded [15].

In this investigation, the development of the surface oxides formed over the first 100 hours of exposure to 800 °C has been revealed using SGIXD (Figure 4) showing a gradual formation of various oxides with time. While peaks associated with NiO, $NiCr_2O_4$ (tetragonal), $(Cr_{0.88}Ti_{0.12})_2O_3$, $(Ni,Co)(Cr,Co)_2O_4$, $NiTiO_3$, and $CrTaO_4$ were identified, the peak intensities were relatively low (0-20 hours) until the later stages (80-100 hours) where more reliable identification was possible. The formation of NiO, $NiCr_2O_4$, and $(Ni,Co)(Cr,Co)_2O_4$ was expected and has been reported in similar studies [25,40–45]. This phenomenon is typically attributed to the alloy forming spinels and/or NiO upon initial exposure to air at high temperatures and has been shown by Evangelou et al. [44] to predominate at high oxygen partial pressures. Although the temperatures investigated in [44] were significantly lower than in this study, similar oxidation mechanisms were proposed for the formation of NiO and spinels. Moreover, the formation of $NiCr_2O_4$ may have contributed to decreased oxidation resistance as it has been previously associated with non-protective oxidation behaviour [4].

The detection and formation of $(Cr_{0.88}Ti_{0.12})_2O_3$ is not frequently reported in similar studies [8,11] on RR1000 from 600-900 °C potentially due to the limited resolution of conventional XRD techniques. However, Reynolds et al. [25] reported the formation of this phase at 650 °C for RR1000, which was attributed to a Ti-doped Cr_2O_3 scale. In addition, Wang et al. [46] have also reported the formation of $(Cr_{0.88}Ti_{0.12})_2O_3$ in the GH4720Li Ni-based superalloy at temperatures ranging from 750-900 °C. The effect of Ti-doping on the Cr_2O_3 scale in Ni-based alloys has also been previously reported by several researchers [8,11–14] therefore its occurrence in this study is expected given the Ti concentration of RR1000. The use of SGIXD has thus been able to provide a more detailed investigation of the oxides formed even at short thermal exposures providing greater detail of this important stage in the oxidation process. Similarly, $NiTiO_3$ (nickel titanate) is seldom observed, however, its formation is speculated to result from a chemical reaction between NiO and TiO_2, as shown in the reaction quoted in Equation 2 [47–49]. When detected, $NiTiO_3$ has been associated with a fast-growing and non-protective scale [48]. In addition, several other reactions are possible that would result in a decrease and subsequent disappearance of the initially formed NiO. These include:

$$NiO\ (s) + TiO_2\ (s) = NiTiO_3\ (s) \qquad\qquad (2)$$

$$NiO\ (s) + Cr_2O_3\ (s) = NiCr_2O_4\ (s) \qquad\qquad (3)$$

$$4NiO\ (s) + 2Cr\ (s) = NiCr_2O_4\ (s) + 3Ni\ (s) \qquad\qquad (4)$$

$$2NiO\ (s) + 4Cr\ (s) + 3O_2\ (g) = 2NiCr_2O_4\ (s) \qquad\qquad (5)$$
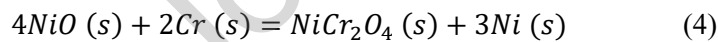
where s indicates a solid phase and g indicates a gaseous phase. Equations (2), (3), and (4) are solid-state reactions with no associated mass change, while reaction (5) would result in a change of mass.

The increasing Ta concentrations on the surface in Figure 7 are consistent with the detection of $CrTaO_4$ in the SGIXD results. The identification of Ta-rich particles in the oxide layer is consistent with Das et al. [40] who observed Ta-rich oxide particles in the superalloy CM-247LC after exposure at 1000-1200 °C. The occurrence of $CrTaO_4$ aligns well with previous studies [43,50,51] where complex oxides of the form (Cr, Ti, Al)(Ta, Ti)O_4 tend to form at temperatures below 1100 °C. Pieraggi et al. [51] surmised that $CrTaO_4$ can form a continuous solid solution with rutile TiO_2 given that $CrTaO_4$ also possesses a rutile structure. Indeed, the addition of Ta was shown to be beneficial for the oxidation performance of Co-Cr-Ta alloys by Irving et al. [52]. It has also been reported by Jalowicka et al. [15] that Ta and Ti can react with oxygen to form

TiTaO$_4$, which reduces Ti-doping of Cr$_2$O$_3$ and promotes dense Al$_2$O$_3$ sub-scale formation. However, it is noted that the alloys in that work (Rene 80 and PWA 1483) had significantly higher Ti and Ta concentrations than RR1000, which prevents a direct comparison. No evidence of Ta$_2$O$_5$ was detected in this study, contrasting to studies undertaken at different temperatures [43,53]. However, it can be inferred from the work of Ren et al. [50] that Ta$_2$O$_5$ may initially form as a precursor oxide that subsequently reacts with Cr$_2$O$_3$ to form CrTaO$_4$. It is therefore possible that any Ta$_2$O$_5$ that may have formed in RR1000 was rapidly developed into CrTaO$_4$. The absence of NiTa$_2$O$_6$ tri-rutiles in RR1000 differs from the work of Nychka et al. [42] which is likely due to PWA 1484 having a much higher Ta concentration.

In general, the SGIXD data (Figure 4) shows that the Cr$_2$O$_3$ peaks become much more prominent after 40 hours, aligning well with the TGA data where the specific mass change curve begins to adopt a parabolic profile. This agreement suggests that the onset of transient oxidation and the shift towards dominance of a specific oxide (e.g. Cr$_2$O$_3$) could be monitored with the use of TGA experiments alone.

To summarise, it is proposed that the oxidation behaviour of RR1000 at 800 °C could be broadly divided into two stages: early and late. The early stage, up to 40 hours, was characterised by approximately linear growth kinetics with the initial formation of NiO, during the heating stage, followed by a mixture of spinels (NiCr$_2$O$_4$/(Ni,Co)(Cr,Co)$_2$O$_4$) and Cr$_2$O$_3$/(Cr$_{0.88}$Ti$_{0.12}$)$_2$O$_3$ and other minor oxide phases, without a clear oxide preference. The formation of NiO subsided due to competing oxide formation and participation in chemical reactions. As discussed in the literature, the spinels and (Cr$_{0.88}$Ti$_{0.12}$)$_2$O$_3$ in the early stage could have acted as barriers to oxygen ingress [27], which may have facilitated the formation of Cr$_2$O$_3$ and some TiO$_2$. In the late stage, from 40 hours onward, Cr$_2$O$_3$ emerged as the dominant oxide as well as the continued formation of TiO$_2$. In addition, the formation of spinels decreased while relatively small levels of NiTiO$_3$ and CrTaO$_4$ remained. It was shown in this study that oxide phase characterisation during the transient oxidation regime was enabled using the high intensity and angular resolution of SGIXD, which was subsequently able to rationalise the pseudo-linear oxidation kinetics.

5 Conclusions

In this study, three techniques were used to characterise the transient oxidation behaviour of the commercial polycrystalline Ni-based superalloy, RR1000, in air at 800 °C from 0-100 hours. The main findings are as follows:

- RR1000 exhibited approximately linear specific mass change kinetics up to approximately 40 hours of oxidation, beyond which parabolic kinetics was evident. The n and k_n values were 1.286 and 1.623×10^{-3} mg^n/cm^{2n}h, respectively. When fitted to parabolic kinetics, the values compared well to literature data. The changes in kinetics observed in this study were rationalised as an extended period of transient oxidation before a continuous and protective Cr$_2$O$_3$ scale was established.
- A continuous external Cr$_2$O$_3$ scale formed on the surface of RR1000 with internal Al$_2$O$_3$ finger-like intrusions, which is characteristic of the oxidation behaviour for alloys of this chemical composition. TiO$_2$ was also detected at the surface.
- SGIXD results showed a clear and systematic evolution of oxide spectra with increasing oxidation time. Peaks associated with Cr$_2$O$_3$ and TiO$_2$ increased in intensity with increasing time at temperature. To a lesser extent, the presence of NiO, NiCr$_2$O$_4$, (Ni,Co)(Cr,Co)$_2$O$_4$, (Cr$_{0.88}$Ti$_{0.12}$)$_2$O$_3$, NiTiO$_3$, and CrTaO$_4$ was also detected.
- Rietveld refinement of the SGIXD data revealed two main stages in the oxidation process of RR1000: The early stage, demonstrated by approximately linear kinetics, was characterised by the formation of NiO during the heating stage followed by the formation of spinels (NiCr$_2$O$_4$/(Ni,Co)(Cr,Co)$_2$O$_4$), and Cr$_2$O$_3$/(Cr$_{0.88}$Ti$_{0.12}$)$_2$O$_3$ and a number of minor oxide phases. The

late stage, from 40 hours onwards, was characterised by the growth of Cr_2O_3 and TiO_2 and the establishment of parabolic oxidation kinetics.

- The extended transient oxidation regime was attributed to the slower heating rate undertaken in this study, which delayed parabolic kinetics in RR1000.

Funding

6   CRediT Authorship Contribution Statement

J. W. X. Wo: Validation, Methodology, Formal Analysis, Investigation, Data Curation, Writing – original draft, Visualization. **D. M. Collins:** Experimentation, Rietveld Analysis, Data Interpretation, Writing – review & editing. **M. P. Taylor:** Conceptualization, Experimentation, Rietveld Analysis, Data Interpretation, Writing – review & editing. **M. C. Hardy:** Resources, Funding Acquisition, Writing – review & editing. **H. J. Stone:** Conceptualization, Supervision, Writing – review & editing, Funding Acquisition, Project Administration.

Declaration of interests

☐ The authors declare that they have no known competing financial interests or personal relationships that could have appeared to influence the work reported in this paper.

☒ The authors declare the following financial interests/personal relationships which may be considered as potential competing interests:

> J.W.X. Wo reports financial support was provided by Rolls-Royce plc. J.W.X. Wo reports financial support was provided by the Natural Sciences and Engineering Research Council of Canada. J.W.X. Wo reports financial support was provided by the Cambridge trusts. H.J. Stone reports a relationship with Rolls-Royce plc that includes: consulting or advisory.

7   Acknowledgements

Declaration of Generative AI in Scientific Writing

GPT-3, OpenAI's large-scale language-generation model (ChatGPT), was used in the writing process to check grammar and improve conciseness. J.W.X. Wo reviewed, edited, and revised all text that was

generated by ChatGPT to his satisfaction and the authors take ultimate responsibility for the content of this publication.

8 Data Availability

The underlying research data required to reproduce these findings are available from the University of Cambridge repository (https://doi.org/10.17863/CAM.97061) [54].

9 References

[1]   A. Kracke, Superalloys, the Most Successful Alloy System of Modern Times-Past, Present, and Future, in: 7th International Symposium on Superalloy 718 and Derivatives, 2010: pp. 13–50.

[2]   J.H. Chen, P.M. Rogers, J.A. Little, Oxidation behavior of several chromia-forming commercial nickel-base superalloys, Oxidation of Metals. 47 (1997) 381–410.

[3]   A. Chyrkin, P. Huczkowski, V. Shemet, L. Singheiser, W.J. Quadakkers, Sub-Scale Depletion and Enrichment Processes During High Temperature Oxidation of the Nickel Base Alloy 625 in the Temperature Range 900-1000 °C, Oxidation of Metals. 75 (2011) 143–166.

[4]   C. Giggins, F. Pettit, Oxidation of Ni-Cr-Al Alloys Between 1000° and 1200°C, J Electrochem Soc. 118 (1971) 1782–1790.

[5]   K.A. Christofidou, N.G. Jones, M.C. Hardy, H.J. Stone, The Oxidation Behaviour of Alloys Based on the Ni–Co–Al–Ti–Cr System, Oxidation of Metals. 85 (2016) 443–458.

[6]   S. Cruchley, M.P. Taylor, H.E. Evans, M.C. Hardy, D.J. Child, Characterisation of subsurface oxidation damage in Ni based superalloy, RR1000, Materials Science and Technology. 30 (2014) 1884–1889.

[7]   S. Cruchley, M.P. Taylor, H.E. Evans, P. Bowen, M.C. Hardy, S. Stekovic, Microstructural Characterisation of High Temperature Oxidation of Nickel Base Superalloy RR1000 and the Effect of Shot-Peening, Superalloys 2012. (2012) 751–758.

[8]   S. Cruchley, H.E. Evans, M.P. Taylor, M.C. Hardy, S. Stekovic, Chromia layer growth on a Ni-based superalloy: Sub-parabolic kinetics and the role of titanium, Corros Sci. 75 (2013) 58–66.

[9]   M.P. Taylor, H.E. Evans, S. Stekovic, M.C. Hardy, The oxidation characteristics of the nickel-based superalloy, RR1000, at temperatures of 700-900°C, Materials at High Temperatures. 29 (2012) 145–150.

[10]   F. Ismail, V. Vorontsov, T. Lindley, M. Hardy, D. Dye, B. Shollock, Alloying effects on oxidation mechanisms in polycrystalline Co–Ni base superalloys, Corros Sci. 116 (2017) 44–52.

[11]   S. Cruchley, M.P. Taylor, R. Ding, H.E. Evans, D.J. Child, M.C. Hardy, Comparison of Chromia Growth Kinetics in a Ni-based Superalloy, with and without Shot-peening, Corros Sci. 100 (2015) 242–252.

[12]   K. Wollgarten, T. Galiullin, W.J. Nowak, W.J. Quadakkers, D. Naumenko, Effect of alloying additions and presence of water vapour on short-term air oxidation behaviour of cast Ni-base superalloys, Corros Sci. 173 (2020) 1–11.

[13]   H. Nagai, M. Okabayashi, Deleterious Effect of Ti Addition on the Oxidation Resistance of Ni-20Cr Alloy, Transactions of the Japan Institute of Metals. 22 (1981) 691–698.

[14]   A. Atkinson, M.R. Levy, S. Roche, R.A. Rudkin, Defect properties of Ti-doped Cr2O3, Solid State Ion. 177 (2006) 1767–1770.

[15]   A. Jalowicka, W. Nowak, D. Naumenko, L. Singheiser, W. Quadakkers, Effect of nickel base superalloy composition on oxidation resistance in SO2 containing, high pO2 environments, Materials and Corrosion. 65 (2014) 178–187.

[16]   M. Taylor, R. Ding, P. Mignanelli, M. Hardy, Oxidation behaviour of a developmental nickel-based alloy and the role of minor elements, Corros Sci. 196 (2022) 110002.

[17]   G.C. Wood, B. Chattopadhyay, Transient oxidation of Ni-base alloys, Corros Sci. 10 (1970) 471–480.

[18]   L. Luo, L. Zou, D.K. Schreiber, D.R. Baer, S.M. Bruemmer, G. Zhou, C.M. Wang, In-situ transmission electron microscopy study of surface oxidation for Ni–10Cr and Ni–20Cr alloys, Scr Mater. 114 (2016) 129–132.

[19]   R. Ramanathan, G. Ramalingam, J.H. Perepezko, P. Reinke, P.W. Voorhees, Evolution of NiO Island Size Distributions during the Oxidation of a Ni-5Cr Alloy: Experiment and Modeling, American Chemical Society Applied Materials and Interfaces. 10 (2018) 9136–9146.

[20]   W.H. Blades, P. Reinke, From Alloy to Oxide: Capturing the Early Stages of Oxidation on Ni-Cr(100) Alloys, American Chemical Society Applied Materials and Interfaces. 10 (2018) 43219–43229.

[21]   H. Hindam, D. Whittle, Microstructure, Adhesion and Growth Kinetics of Protective Scales on Metals and Alloys, Oxidation of Metals. 18 (1982) 245–285.

[22]   J.L. Smialek, P.J. Bonacuse, Compositional effects on the cyclic oxidation resistance of conventional superalloys, Materials at High Temperatures. 33 (2016) 489–500.

[23]   G. Calvarin, R. Molins, A.M. Huntz, Oxidation Mechanism of Ni-20Cr Foils and Its Relation to the Oxide-Scale Microstructure, Oxidation of Metals. 53 (2000) 25–48.

[24]   X.X. Yu, A. Gulec, Q. Sherman, K.L. Cwalina, J.R. Scully, J.H. Perepezko, P.W. Voorhees, L.D. Marks, Nonequilibrium Solute Capture in Passivating Oxide Films, Phys Rev Lett. 121 (2018) 145701–145702.

[25]   T.D. Reynolds, D.M. Collins, N.K. Soor, S.R. Street, N. Warnken, P.M. Mignanelli, M.C. Hardy, H.E. Evans, M.P. Taylor, Identifying heating rate dependent oxidation reactions on a nickel-based superalloy using synchrotron diffraction, Acta Mater. 181 (2019) 570–583.

[26]   C. Greskovich, Kinetics of NiCr2O4 Formation and Diffusion of Cr3+ Ions in NiO, Journal of the American Ceramic Society. 53 (1970) 498–502.

[27]   M.H. Li, X.F. Sun, J.G. Li, Z.Y. Zhang, T. Jin, H.R. Guan, Z.Q. Hu, Oxidation Behavior of a Single-Crystal Ni-Base Superalloy in Air. I: At 800 and 900°C, Oxidation of Metals. 59 (2003) 591–605.

[28] T.D. Reynolds, M.P. Taylor, D.J. Child, H.E. Evans, The effect of elevated air pressure on the oxidation properties of the nickel-based superalloy, RR1000, at 650°C with different surface modifications, Materials at High Temperatures. 35 (2018) 130–140.

[29] M.P. Taylor, D. Calderwood, T.D. Reynolds, N. Warnken, P.M. Mignanelli, M.C. Hardy, D.M. Collins, Temperature Range of Heating Rate Dependent Reactions Leading to Spinel Formation on a Ni-Based Superalloy, High Temperature Corrosion of Materials. (2023) 1–19.

[30] D. Monceau, B. Pieraggi, Determination of Parabolic Rate Constants from a Local Analysis of Mass-Gain Curves, Oxidation of Metals. 50 (1998).

[31] A.J. Goodfellow, E.I. Galindo-Nava, C. Schwalbe, H.J. Stone, The role of composition on the extent of individual strengthening mechanisms in polycrystalline Ni-based superalloys, Mater Des. 173 (2019) 1–15.

[32] A.J. Manning, D. Knowles, C.J. Small, European Patent Specification EP 1 193 321 B1, 2003.

[33] A.A. Coelho, TOPAS and TOPAS-Academic: an optimization program integrating computer algebra and crystallographic objects written in C++, J Appl Crystallogr. 51 (2018) 210–218.

[34] FIZ Karlsruhe GmbH, Inorganic Crystal Structure Database (ICSD), 1985.

[35] A. Encinas-Oropesa, G.L. Drew, M.C. Hardy, A.J. Leggett, J.R. Nicholls, N.J. Simms, Effects of Oxidation and Hot Corrosion in a Nickel Disc Alloy, Superalloys. (2008) 609–618.

[36] G. Ueno, S. Sato, Y. Kino, The low-temperature tetragonal phase of $NiCr_2O_4$, Acta Crystallogr. C55 (1999) 1963–1966.

[37] W.J. Nowak, Effect of Surface Roughness on Early Stage Oxidation Behavior of Ni-Base Superalloy IN 625, Applied System Innovation 2018, Vol. 1, Page 32. 1 (2018) 32.

[38] K. Fujiwara, Z. Horita, Measurement of intrinsic diffusion coefficients of Al and Ni in Ni_3Al using Ni/NiAl diffusion couples, Acta Mater. 50 (2002) 1571–1579.

[39] J.W.X. Wo, H.T. Pang, A.S. Wilson, M.C. Hardy, H.J. Stone, The Isothermal Oxidation of a New Polycrystalline Turbine Disk Ni-Based Superalloy at 800 °C and Its Modification with Pre-oxidation, Metallurgical and Materials Transactions A. (2022) 1–15.

[40] D.K. Das, V. Singh, S. V. Joshi, High temperature oxidation behaviour of directionally solidified nickel base superalloy CM - 247LC, Materials Science and Technology. 19 (2003) 695–708.

[41] H.T. Mallikarjuna, N.L. Richards, W.F. Caley, Isothermal Oxidation Comparison of Three Ni-Based Superalloys, J Mater Eng Perform. 26 (2017) 2014–2023.

[42] J.A. Nychka, D.R. Clarke, G.H. Meier, Spallation and transient oxide growth on PWA 1484 superalloy, Materials Science and Engineering: A. 490 (2008) 359–368.

[43] K. Rehman, N. Sheng, Z. Sang, S. Xun, Z. Wang, J. Xie, G. Hou, Y. Zhou, X. Sun, Comparative study of the reactive elements effects on oxidation behavior of a Ni-based superalloy, Vacuum. 191 (2021) 110382.

[44] A. Evangelou, K.A. Soady, S. Lockyer, N. Gao, P.A.S. Reed, Oxidation behaviour of single crystal nickel-based superalloys: intermediate temperature effects at 450–550°C, Materials Science and Technology (United Kingdom). 34 (2018) 1679–1692.

[45]   T.S. Sidhu, S. Prakash, R.D. Agrawal, Hot corrosion resistance of high-velocity oxyfuel sprayed coatings on a nickel-base superalloy in molten salt environment, Journal of Thermal Spray Technology. 15 (2006) 387–399.

[46]   M. Wang, J. Qu, T. Yin, J. Sheng, Q. Deng, Lu X, Study on Oxidation Behaviour of Alloy GH4720Li at High Temperatures, Journal of Iron and Steel Research. 22 (2010) 28–33.

[47]   C.E. Lowell, H.B. Probst, NASA Technical Note: Effects of Composition and Testing Conditions on Oxidation Behavior of Four Cast Commercial Nickel-Base Superalloys, 1974.

[48]   J. Smialek, A. Garg, T. Gabb, R. MacKay, Cyclic Oxidation of High Mo, Reduced Density Superalloys, Metals (Basel). 5 (2015) 2165–2185.

[49]   P. Song, M. Liu, X. Jiang, Y. Feng, J. Wu, G. Zhang, D. Wang, J. Dong, X.Q. Chen, L. Lou, Influence of alloying elements on hot corrosion resistance of nickel-based single crystal superalloys coated with Na2SO4 salt at 900 °C, Mater Des. 197 (2021) 1–12.

[50]   W. Ren, F. Ouyang, B. Ding, Y. Zhong, J. Yu, Z. Ren, L. Zhou, The influence of CrTaO4 layer on the oxidation behavior of a directionally-solidified nickel-based superalloy at 850–900 °C, J Alloys Compd. 724 (2017) 565–574.

[51]   B. Pieraggi, F. Dabosi, High-temperature oxidation of a single crystal Ni-base superalloy, Materials and Corrosion. 38 (1987) 584–590.

[52]   G.N. Irving, J. Stringer, D.P. Whittle, The oxidation of Co-20% Cr base alloys containing Nb or Ta, Corros Sci. 15 (1975) 337–344.

[53]   Y.B. Hu, C.Q. Cheng, T.S. Cao, L. Zhang, J. Zhao, New sight on the oxide film growth mechanism in a single crystal Ni-based superalloy with a ground surface signature, Corros Sci. 199 (2022) 110173.

[54]   J.W.X. Wo, D.M. Collins, M.P. Taylor, M.C. Hardy, H.J. Stone, Research Data Supporting "Delayed Parabolic Oxidation via Transient Thermal Exposures on a Polycrystalline Nickel-Based Superalloy." https://doi.org/10.17863/CAM.97061.

Highlights

- Multiple oxides form during transient oxidation, prior to Cr_2O_3, on a Ni-superalloy
- Transient effects are evident up to 40 hours of isothermal exposure at 800 °C
- Early pseudo-linear kinetics governed by NiO and $NiCr_2O_4$/(Ni,Co)(Cr,Co)$_2O_4$ growth
- Late-stage parabolic kinetics dominated by Cr_2O_3, $(Cr_{0.88}Ti_{0.12})_2O_3$, and TiO_2
- Cr_2O_3 emerges as the dominant passivating oxide